International Journal of Pharmaceutics 584 (2020) 119409

Contents lists available at ScienceDirect

International Journal of Pharmaceutics

journal homepage: www.elsevier.com/locate/ijpharm

Systematic evaluation of design features enables efficient selection of Π electron-stabilized polymeric micelles

Maryam Sheybanifard[a,1], Nataliia Beztsinna[b,1], Mahsa Bagheri[b], Eva Miriam Buhl[c], Jaleesa Bresseleers[d,e], Aida Varela-Moreira[b,f], Yang Shi[a], Cornelus F. van Nostrum[b], Gabri van der Pluijm[g], Gert Storm[b,h], Wim E. Hennink[b], Twan Lammers[a,b,h], Josbert M. Metselaar[a,h,*]

[a] Department of Nanomedicine and Theranostics, Institute for Experimental Molecular Imaging, Uniklinik RWTH Aachen and Helmholtz Institute for Biomedical Engineering, Faculty of Medicine, RWTH Aachen University, 52074 Aachen, Germany
[b] Department of Pharmaceutics, Utrecht Institute for Pharmaceutical Sciences (UIPS), Faculty of Science, Utrecht University, 3508 TB Utrecht, the Netherlands
[c] Electron Microscopy Facility, Institute of Pathology, RWTH University Hospital, Aachen, Germany
[d] ChemConnection BV – Ardena Oss, 5349 AB Oss, the Netherlands
[e] Department of Bio-Organic Chemistry, Eindhoven University of Technology, 5600 MB Eindhoven, the Netherlands
[f] Laboratory of Clinical Chemistry and Hematology (LKCH), University Medical Center Utrecht, Heidelberglaan 100, 3584 CX Utrecht, the Netherlands
[g] Leiden University Medical Center, Department of Urology, J-3-108, Albinusdreef 2, 2333 ZA Leiden, the Netherlands
[h] Department of Biomaterials Science and Technology, MIRA Institute for Biomedical Technology and Technical Medicine, University of Twente, Enschede, the Netherlands

ARTICLE INFO

Keywords:
Polymeric micelles
π-π stacking interactions
Paclitaxel
In vitro release kinetics
3D cell culture
Storage stability

ABSTRACT

Polymeric micelles (PM) based on poly(ethylene glycol)-*b*-poly(*N*-2-benzoyloxypropyl methacrylamide) (mPEG-*b*-p(HPMA-Bz)) loaded with paclitaxel (PTX-PM) have shown promising results in overcoming the suboptimal efficacy/toxicity profile of paclitaxel. To get insight into the stability of PTX-PM formulations upon storage and to optimize their *in vivo* tumor-targeted drug delivery properties, we set out to identify a lead PTX-PM formulation with the optimal polymer composition. To this end, PM based on four different $mPEG_{5k}$-*b*-p(HPMA-Bz) block copolymers with varying molecular weight of the hydrophobic block (17–3 kDa) were loaded with different amounts of PTX. The hydrodynamic diameter was 52 ± 1 nm for PM prepared using polymers with longer hydrophobic blocks ($mPEG_{5k}$-*b*-$p(HPMA\text{-}Bz)_{17k}$ and $mPEG_{5k}$-*b*-$p(HPMA\text{-}Bz)_{10k}$) and 39 ± 1 nm for PM composed of polymers with shorter hydrophobic blocks ($mPEG_{5k}$-*b*-$p(HPMA\text{-}Bz)_{5k}$ and $mPEG_{5k}$-*b*-$p(HPMA\text{-}Bz)_{3k}$). The best storage stability and the slowest PTX release was observed for PM with larger hydrophobic blocks. On the other hand, smaller sized PM of shorter $mPEG_{5k}$-*b*-$p(HPMA\text{-}Bz)_{5k}$ showed a better tumor penetration in 3D spheroids. Considering better drug retention capacity of the $mPEG_{5k}$-*b*-$p(HPMA\text{-}Bz)_{17k}$ and smaller size of the $mPEG_{5k}$-*b*-$p(HPMA\text{-}Bz)_{5k}$ as two desirable design features, we argue that PM based on these two polymers are the lead candidates for further *in vivo* studies.

1. Introduction

Paclitaxel (PTX) is an established and potent chemotherapeutic drug used as standard of care for multiple types of cancer such as prostate, ovarian, breast, and lung cancer (Desai et al., 2006; Jordan et al., 1996; Kim et al., 2001). However, the chemical nature of PTX leads to suboptimal biodistribution and insufficient target site accumulation. Hence, improving its pharmacokinetic profile and maximizing its anticancer effect is of great importance (Cragg, 1998).

Various attempts have been made to overcome these limitations. To address its poor water solubility, Taxol® was introduced as a commercially available formulation of PTX utilizing Cremophor EL and dehydrated ethanol (1:1, v/v) as excipients (Adams et al., 1993). Clinical studies however, showed that Cremophor EL can cause an extensive range of adverse effects (Peltier et al., 2006; van Zuylen et al., 2001) such as acute hypersensitivity reactions and neurological toxicity (Gelderblom et al., 2001). Moreover, premedication is required to manage these adverse reactions (Finley and Rowinsky, 1994), which

* Corresponding author at: Department of Nanomedicine and Theranostics, Institute for Experimental Molecular Imaging, Uniklinik RWTH Aachen and Helmholtz Institute for Biomedical Engineering, Faculty of Medicine, RWTH Aachen University, 52074 Aachen, Germany.
E-mail address: jmetselaar@ukaachen.de (J.M. Metselaar).
[1] These authors contributed equally to this work.

https://doi.org/10.1016/j.ijpharm.2020.119409
Received 29 February 2020; Received in revised form 3 May 2020; Accepted 4 May 2020
Available online 07 May 2020
0378-5173/

can be accompanied by additional side effects (Quock et al., 2002). Therefore, improved tumor-targeted delivery of PTX requires nanocarrier formulations that sufficiently retain the drug while circulating in the bloodstream upon intravenous administration and release the drug at the target site. To this end, Abraxane® was introduced as a next-generation nanoparticulate formulation of PTX which is approved by the US Food and Drug Association (US FDA) and European Medicines Agency (EMA). In this formulation, albumin-PTX nanoparticles are prepared through high-pressure homogenization method and avoid the Cremophor-associated adverse effects (Blum et al., 2004; Ibrahim et al., 2002). Nevertheless, the nanoformulation generated with albumin suffers from instability issues post injection. It has been shown that upon dilution in the bloodstream, 130 nm-sized nanoparticles break down into 10 nm soluble albumin-PTX components (Chauhan et al., 2012).

In the search for better formulations of PTX, polymeric micelles (PM) appear to be an attractive approach (Cabral et al., 2018; Nishiyama et al., 2016; Soga et al., 2005). In 1980s, Ringsdorf and colleagues introduced PM as a potential drug delivery system (Bader et al., 1984; Pratten et al., 1985). Since then, PM have been shown to successfully deliver many drugs of interest (Hamaguchi et al., 2005; Kim et al., 2004; Talelli et al., 2010; Yoo and Park, 2001). PM are formed by self-assembly of amphiphilic block copolymers in aqueous media. The inner core of PM consists of the hydrophobic blocks of the block copolymers, which makes it suitable to solubilize hydrophobic compounds. The outer shell of PM is formed by the hydrophilic blocks of the block copolymer, which stabilizes the system in aqueous environments (Nasongkla et al., 2006; Shiraishi and Yokoyama, 2013; Soga et al., 2005; Yokoyama, 2014). Besides solubility enhancement, PM allow for surface modification, which can be used to prolong blood circulation time or achieve tumor targeting (Deng et al., 2012). PM enable tumor targeted drug delivery through the enhanced permeability and retention (EPR) effect (passive targeting) and/or through the introduction of target-selective ligands (e.g. antibodies, sugar moieties, folate residues, etc.), which enable PM to target specific receptors expressed in tumor tissue via active targeting (Fang et al., 2011; Gothwal et al., 2016; Lu and Park, 2013; Torchilin, 2007). Therefore, exploiting PM can be a promising method to advance PTX therapeutics by overcoming the solubility issue of very hydrophobic drugs, avoiding the use of Cremophore EL and related adverse effects, improving pharmacokinetics and achieving effective tumor-targeted delivery.

A main challenge in polymeric micelle field is to improve the physical instability of PM drug formulations in the blood stream. PM-based drug formulations are known to disassemble below the critical micelle concentration, leading to premature and non-controlled drug release (Letchford et al., 2009; Miller et al., 2013; Shi et al., 2017; Shi et al., 2015). To resolve this issue, core-crosslinking of PM has been explored (Kim et al., 1999; Shuai et al., 2004; van Nostrum, 2011). Nevertheless, in this approach, extra steps are needed to achieve PM stability. Covalent core-crosslinking is normally implemented after PM preparation and also, may not always retain PTX in the micelles effectively (Talelli et al., 2015; Talelli et al., 2012).

An elegant way to improve physical stability of PM and avoid crosslinking is the introduction of non-covalent π-π stacking interactions between aromatic groups of a drug and the hydrophobic block of the micelle-forming polymers. As presented by others, this strategy appeared to present a step forward in enhancing the drug loading capacity and improving PM stability and drug retention (Kataoka et al., 2000; Shi et al., 2013; Zhuang et al., 2019). Exploiting mPEG-*b*-p(HPMA-Bz), Shi et al. designed PTX loaded PM which showed prolonged blood circulation time and excellent antitumor activity and safety in preclinical tumor models (Shi et al., 2015).

After these studies, further improvements have been explored on π electron-stabilized PM. Initially, tetrahydrofuran (THF) was selected as an organic solvent to generate PM (Naksuriya et al., 2015; Shi et al., 2015). Comparison of different organic solvents showed that using ethanol leads to PM with a smaller size (Bagheri et al., 2018). Obtaining smaller-sized nanoparticles is a critical achievement in tumor-targeted drug delivery with researchers suggesting a better tumor penetration, improved intratumoral delivery, and further enhancement of the efficacy as a consequence (Cabral et al., 2011). Moreover, residual THF might result in toxicity (Cooney et al., 1993). Hence, replacing THF with ethanol, which is a rather safe organic solvent, would be more appealing for clinical translation (Guideline, 2005).

In the present study, we systematically investigated possibilities for optimization of PTX-PM to achieve PM with both the smallest size and highest PTX retention. To this end, we used four different $mPEG_{5k}$-*b*-p(HPMA-Bz) block copolymers with a fixed molecular weight of PEG and different molecular weights of the hydrophobic pHPMA-Bz block. Using ethanol as a more pharmaceutically acceptable solvent, we prepared PM with different ratios of drug to excipient. To evaluate the effects of polymer variants and drug to polymer ratio on the size and PTX retention, we performed studies regarding the stability, drug retention and release, cellular uptake and 3D spheroid penetration of the PM.

2. Material and methods

2.1. Materials

PTX was purchased from Biorbyt Ltd, Cambridge, Cambridgeshire, United Kingdom. Slide-A-Lyzer™ cassette (MWCO of 10 kDa) was obtained from Thermo-Fisher Scientific. HEPES was purchased from Sigma Aldrich (Saint Louis, USA). Analytical grade ethanol was purchased from Merck (Darmstadt, Germany) and HPLC-S gradient grade acetonitrile was obtained from Biosolve Chimie SARL (Dieuze, France). Polysorbate 80 (Tween 80®, Fisher Scientific UK, Loughborough, Leicester, UK) and Bovine Serum Albumin (Sigma A-4503) were used as solubilizers of released PTX in the release tests. Spectra/Por® Float-A-Lyzer® G2 dialysis membranes with the MWCO of 100 kDa and 300 kDa were purchased from Spectrum labs (Rancho Dominguez California, USA). All cell labeling reagents and fluorescent dyes were purchased from Thermo Fisher Scientific (Naarden, the Netherlands) unless stated otherwise. Cell medium and supplements were from Gibco BRL Thermo Fisher Scientific (Naarden, the Netherlands).

2.2. Preparation of PM

Four types of $mPEG_{5k}$-*b*-p(HPMA-Bz) polymer were synthesized as described previously (Bagheri et al., 2018). The polymers were synthesized with different molar feed ratios of macro-initiator: monomer to yield $mPEG_{5k}$-*b*-$p(HPMA\text{-}Bz)_{17k}$, $mPEG_{5k}$-*b*-$p(HPMA\text{-}Bz)_{10k}$, $mPEG_{5k}$-*b*-$p(HPMA\text{-}Bz)_{5k}$, and $mPEG_{5k}$-*b*-$p(HPMA\text{-}Bz)_{3k}$. In order to prepare PM, variable amounts of PTX (1.5, 3 and 4.5 mg PTX), were added to 1 mL solution of 30 mg/mL of the polymer in ethanol while heating at 60 °C. After complete dissolution, the organic phase was added to 1 mL of HEPES Buffered Saline (HBS 1x, HEPES 20 mM and NaCl 150 mM, pH 7.4) while heating at 60 °C and stirring (200–400 rpm) for 1–2 min. PM formulations were placed in a dialysis cassette (MWCO of 10 kDa) at the room temperature to dialyze against HBS for 48 h. The PTX-PM formulations were filtered through 0.45 μm filters to remove unencapsulated fraction (precipitations) of the drug.

2.3. Characterization of PM

2.3.1. Dynamic light scattering and PM morphology

The hydrodynamic diameter (Z-ave) of the formed PM was measured utilizing Dynamic Light Scattering (DLS, Nano-s, Malvern Instruments Ltd., UK) at room temperature and diluted 10 fold with HBS 1x (if needed). To measure the zeta potential, 1 volume of PM formulation was diluted with 10 volumes of a solution of HEPES (10 mM, pH 7.5) and analyzed with Zetasizer (Nano ZS, Malvern Instruments Ltd., UK). Here, independent replicates were prepared.

Each of the replicates represents an individual formulation which was separately prepared and measured. For transmission electron microscopy (TEM) analysis, samples were allowed to adsorb on glow discharged formvar-carbon-coated nickel grids (Maxtaform, 200 mesh, Plano, Wetzlar, Germany) for 10 min. Negative staining was performed with 0.5% uranyl acetate (Science Services GmbH, Munich, Germany). Samples were examined using a TEM LEO 906 (Carl Zeiss, Oberkochen, Germany), operating at an acceleration voltage of 60 kV.

2.3.2. Determination of the drug encapsulation efficiency and loading capacity using UPLC analysis

A Waters Acquity UPLC system (Waters, MA, USA) was used to quantify PTX concentrations. The method used to measure the PTX concentrations of the different samples was isocratic elution UPLC, with acetonitrile (ACN)/water (H_2O) (45/55 v/v) and 0.1% formic acid as the mobile phase. The injection volume was 2 μL with 1 mL/min flow rate and run time of 1.5 min using the Acquity UPLC BEH C18 column (2.1 mm × 50 mm, 1.7 μm) as the stationary phase. The UV/Vis detector was set at 227 nm and peak integration was done with chromatographic Empower® software. PTX concentrations were calculated using a standard calibration curve. The encapsulation efficiency (EE) and loading capacity (LC) of PTX were calculated as follows:

$$EE\% = \text{Encapsulated drug (after filtration)/initial amount of added drug} * 100\%$$

$$LC\% = \text{Encapsulated drug (after filtration)} /(\text{initial amount of drug + polymer}) * 100\%$$

Here, independent replicates were prepared. Each of the replicates represents an individual formulation which was separately prepared and measured.

2.4. Stability of the PTX-loaded PM

The stability of the different PM was studied by measuring the size and the percentage of remained loaded PTX at different temperatures (7 days at 37 and up to 5 weeks at 25 and 4 °C). PTX-loaded PM were prepared with 30 mg/mL of polymer and drug to polymer ratios of 0.05, 0.1, and 0.15 w/w and without further modifications, were incubated at above mentioned temperatures. To determine the remained loaded drug, samples were centrifuged at 5,000 g for 10 min to separate the precipitated drug from the PM. After centrifugation, a fraction of the supernatant was dissolved in ACN and later measured by UPLC. Here, technical repeats are reported. These repeats were generated by taking samples from one incubated formulation. Similar experiment was conducted to assess the size stability of the PM. After centrifugation, a fraction of the supernatant was used to track the changes in average PM size. Here, independent replicates were prepared. Each of the replicates represents an individual formulation which was separately incubated and measured with DLS.

2.5. Release of PTX from PM in presence of Tween 80®/PBS and BSA/PBS

The release studies were conducted on PTX loaded formulations in phosphate-buffered saline (PBS, pH 7.4 composed of NaCl 137 mM, KCl 2.7 mM, Na_2HPO_4 10 mM, and KH_2PO_4 1.8 mM) containing 0.2% v/v Tween 80® or 4.5% Bovine Serum Albumin (BSA). Prior to release, PTX solubility in PBS with 0.2% Tween 80® was determined by applying different amounts of PTX (0.6, 1.2, and 2.4 mg) in 1 mL of the medium following an incubation at 37 °C for 24 h while agitating. Samples were centrifuged at 10,000 rpm for 20 min to separate the un-dissolved fraction of PTX from the solubilized PTX fraction. Next, 1 volume of the supernatant was diluted with 10 volumes of ACN, centrifuged again at 5,000 g for 10 min and the supernatant was analyzed with UPLC. After determination of PTX solubility in the medium, the required volume of the outer medium was calculated in order to present an excessive amount of Tween 80® in the buffer (Abouelmagd et al., 2015). To confirm the absence of the mixed micelles, a solution of 0.2% Tween 80® micelles was incubated at 37 °C with PM of polymer $mPEG_{5k}$-*b*-p$(HPMA\text{-}Bz)_{17k}$ (30 mg/mL of the polymer) loaded with initial drug/polymer (w/w) ratio of 0.1. Sampling was performed after 1 h, 6 h and daily till 7 days and checked with DLS.

To perform the release study, samples were placed in Float-A-Lyzer® G2 dialysis membrane (MWCO of 100 kDa or 300 kDa). The dialysis bag was submerged in 50 mL of PBS + 0.2% Tween 80® and incubated at 37 °C under gentle agitation and the outer medium was changed regularly. Sampling was performed frequently from inside the membrane for 7 days. At the end of the experiment, samples were diluted with at least 2 volumes of ACN and the concentration of remained encapsulated PTX was measured with UPLC.

To assess the PTX release in BSA, 45 mg/mL solution of BSA in PBS was prepared. 1 volume of the PM was diluted with BSA (2–3 volumes) and placed inside the dialysis membrane. The release study was performed in line with the protocol for the release in PBS + 0.2% Tween 80®. To measure the retained PTX with UPLC, removal of BSA inside the membrane was needed. To this end, 5 volumes of methanol were added to 1 volume of the different samples following by centrifugation at 4,000 rpm for 15 min to remove precipitated BSA. Afterwards, the supernatant was transferred into clean tubes dried under the vacuum rotator. Finally, PTX precipitates were dissolved in ACN and measured by UPLC. In this experiment, independent replicates were prepared. Each of the replicates represents an individual sample which was separately studied for PTX release.

2.6. Cell culture and Cy-labeled PM preparation

Human hepatocellular carcinoma cells (HepG2) were obtained from American Type Culture Collection (ATCC) and cultured in DMEM low glucose medium (Sigma Aldrich) supplemented with 10% FBS (Sigma Aldrich). Human prostate cancer cells (PC3) were obtained from American Type Culture Collection (ATCC) and cultured in McCoy's 5A medium (Sigma Aldrich) supplemented with 10% FBS (Sigma Aldrich). All cells were maintained at 37 °C in a 5% CO_2 and humidified atmosphere. PM used for the uptake and penetration studies were labeled by addition of either Cy3- or Cy5-conjugated polymer (1–3.3% w/w) to the unlabeled polymer. The dye-conjugated polymer was synthesized as described previously (Shi et al., 2015) and the PM were prepared as described in Section 2.2.

2.6.1. PM uptake in 2D

Cells were seeded into 96-well μClear® black plates (Greiner Bio-One, 10,000 cells/ well) and incubated overnight. Next, the medium was replaced with fresh complete medium and appropriate amounts of the PM was added. The cells were incubated with fluorescently labeled PM (using cyanine dyes) and imaged live with 60x objective of CV7000s (Yokogawa Electric Corporation, Tokyo, Japan) as often and as long as it was required for a particular experiment. Non-treated cells were used as negative control. Labeling of the subcellular structures was performed according to the manufacturer instructions. Briefly, for the nuclei staining, the cells were incubated with 10 nM Hoechst 33,342 in PBS (100 μL) for 10 min at 37 °C. The endosomes were stained with pHrodo™ Green Dextran conjugate diluted in complete growth medium to a final concentration of 0.05 mg/mL for 20 min at 37 °C. In this experiment, independent replicates were prepared. Each of the replicates represents an individual cell-cultured well, which was separately measured.

2.6.2. PM penetration in 3D

For the microspheroids generation, HepG2 cells were seeded in Elplasia™ (Kurarray Co Ltd., Japan) microwell plates (20,000 cells/well). The plates are made in 96 well plate format with a microgrid of 200x200 μm squares in the bottom of each well. After seeding, cells were randomly distributed between the squares of the microgrid and formed individual microspheroids in suspension with a diameter of 50–120 μm after 3–5 days of culturing at 37 °C in a 5% CO_2 and humidified atmosphere. Before the addition of PM, cell nuclei of microspheroids were stained with 10 nM Hoechst 33,342 in full culture medium (100 μL) for 1 h at 37 °C. Then, 50% of the medium was replaced with fresh complete medium and appropriate amount of fluorescently labeled PM was added. PM penetration in microspheroids was monitored with 20x objective of CV7000s (Yokogawa Electric Corporation, Tokyo, Japan) as often and as long as it was required for a particular experiment. Non-treated microspheroids were used as negative control.

For the gel penetration study in 3D, 2 lane Mimetas OrganoPlate® (Leiden, the Netherlands) were used. The plates are based on a 384-well microtiter plate format featuring 96 microfluidic tissue chips, with each chip connecting four neighboring wells: one well is used for administering the cell/gel mixture (gel channel, Fig. 7), two wells for supplying growth medium (perfusion channel, Fig. 7), and a fourth well for imaging. The cell/gel mixture fills gel channel of the tissue chip using capillary pressure barriers called phase guides, which provides membrane-free exchange of nutrients, gases, and waste products between the cell/gel and the medium (Wevers et al., 2016).

Here, HepG2 cells were seeded in Mimetas OrganoPlate® in accordance with manufacturer protocols. Briefly, cells were harvested, counted, centrifuged and the pellet was dissolved in Matrigel® (Corning ®, Lot number 7079007, 9.4 mg/mL) at 10^6 cells/mL. Next, 2 μL of gel mixture per chip was pipetted in the gel inlet of the OrganoPlate®. The gel was left to polymerize for 30 min at 37 °C. Afterwards, 50 μL of complete growth medium per chip was pipetted in the medium inlet and the plate was placed on Mimetas rocking platform in the cell incubator to start perfusion (Trietsch et al., 2017). After 3–4 days of growth, the media in each chip were replaced with fresh complete medium with appropriate amount of PM. Before addition of the PM, 10 nM Hoechst 33,342 in complete medium (100 μL) was added for nuclei labeling and incubated for 1 h at 37 °C. After PM addition, the continued gravitational flow was ensured by the Mimetas rocking platform (Trietsch et al., 2017) for 4 or 24 h and subsequently imaged with 10x objective of CV7000s (Yokogawa Electric Corporation, Tokyo, Japan) and the depth of PM perfusion into the gel channel was quantified in 5 gel segments as shown in Fig. 7. Chips with non-treated cells were used as negative control. In this experiment, independent replicates were prepared. Each of the replicates represents an individual cell-cultured well, which was separately measured.

2.6.3. Image analysis

Customized image analysis protocols were developed with Columbus Software (U.S. National Institutes of Health, Bethesda, Maryland, USA). For the gel penetration depth measurements Fiji software was used.

3. Results

3.1. Preparation and characterization of the different mPEG$_{5k}$-b-p(HPMA-Bz) PM

Throughout this study, PM were made from four different mPEG$_{5k}$-*b*-p(HPMA-Bz) block copolymers, with a fixed molecular weight of PEG (5 kDa) and different molecular weights of the hydrophobic blocks of pHPMA-Bz (3, 5, 10 and 17 kDa). Previously, non-drug loaded PM were prepared and their features (such as critical micelle concentration, etc.) were studied (Bagheri et al., 2018). Here, PM of these different polymers loaded with different PTX contents were prepared by nanoprecipitation using ethanol as the solvent for the block copolymers and PTX and HBS as non-solvent. Table 1 reports the loading capacity (LC), encapsulation efficiency (EE), zeta potential, particle size and size distribution of the different PM. This table as well as the data presented in Tables S2 and S3 show that the hydrodynamic diameter (Z-ave) and polydispersity index (PDI) of the PM of a given polymer was not affected by the loading percentage of PTX. However, by decreasing the hydrophobic block size (from 17 to 3 kDa) and thus the hydrophobic/hydrophilic balance of the polymer, the average size of the PM decreased from 53 to 38 nm. The zeta potential of the PM was slightly negative for all variants (between −1.6 and −3.5 mV). The data further show that the EE of PM for PTX ranged from ~40–70% (except for the last formulation of Table S3 (EE was 21%)) resulting in LC's ranging from ~2–9% (Table 1 and Tables S2 and S3).

3.2. Effect of polymer type and drug to polymer ratio on the drug leakage and size stability of PM

In order to assess the performance of PM-based PTX formulations with respect to drug retention during storage, PTX loaded PM were prepared and without further modifications, placed at 37 °C for 7 days. The results show that PM based on mPEG$_{5k}$-*b*-p(HPMA-Bz)$_{3k}$, which contains the shortest hydrophobic polymer block, was by far the leakiest under these conditions (Fig. 1A, S1A and S1C). At the initial drug/polymer ratio of 0.1 this PM retained only 40% of the drug after 6 h of incubation. At 1 day, about 20% of PTX was retained inside these PM while PM based on mPEG$_{5k}$-*b*-p(HPMA-Bz)$_{17k}$ with the longest hydrophobic block still retained almost 80% of PTX. The other two PM formulations showed an intermediate behavior with more PTX leakage from PM prepared of polymer with shorter hydrophobic blocks (i.e. mPEG$_{5k}$-*b*-p(HPMA-Bz)$_{5k}$) (Fig. 1A).

For PM based on mPEG$_{5k}$-*b*-p(HPMA-Bz)$_{17k}$ and mPEG$_{5k}$-*b*-p(HPMA-Bz)$_{3k}$, which are the most and the least stable respectively, drug retention as a function of the initial drug/polymer ratio was assessed. As can be seen in Fig. 1B and C, lower initial drug/polymer ratio clearly led to a better drug retention. As shown in Fig. 1B, the most severe PTX leakage was observed in PM with initial drug/polymer ratio of 0.15 (i.e 15% w/w PTX loading) with 44% of PTX retained inside these PM after 7 days of incubation. In this set, similar drug retention (more than 80%) was observed in PM with initial drug/polymer ratio of 0.05 and 0.1 (i.e 5 and 10% w/w PTX loading). Results showed that PM based on mPEG$_{5k}$-*b*-p(HPMA-Bz)$_{3k}$ with initial drug/polymer ratio of 0.05 (i.e

Table 1
Physicochemical characteristics of PM prepared using block copolymers of different molecular weights with a drug/polymer (w/w) ratio of 0.1 (3 mg PTX and 30 mg polymer). Data are presented as mean ± SD of independent replicates (n = 4).

Polymer	Z-ave (nm)	PDI	Zeta potential* (mV)	EE (%)	LC (%)
mPEG$_{5k}$-b-p(HPMA-Bz)$_{17k}$	53 ± 1	0.05 ± 0.01	−2.1 ± 0.4	52.6 ± 6.7	4.9 ± 0.6
mPEG$_{5k}$-b-p(HPMA-Bz)$_{10k}$	51 ± 1	0.04 ± 0.02	−3.2 ± 1.9	53.9 ± 7.9	5.0 ± 0.6
mPEG$_{5k}$-b-p(HPMA-Bz)$_{5k}$	40 ± 1	0.05 ± 0.03	−3.3 ± 0.7	42.7 ± 8.9	3.9 ± 0.8
mPEG$_{5k}$-b-p(HPMA-Bz)$_{3k}$	38 ± 1	0.10 ± 0.03	−3.1 ± 1.2	43.4 ± 9.2	4.0 ± 1.0

* Zeta potential was measured in a solution of HEPES (10 mM, pH 7.5).

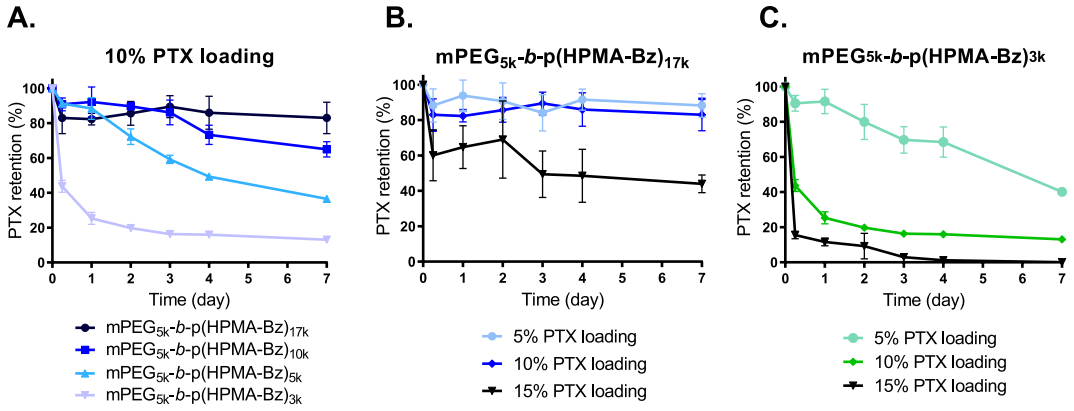

Fig. 1. Drug retention of PM during storage at 37 °C for 7 days in HBS. (A) PM prepared at a drug/polymer ratio of 0.1, (B) PM variant $mPEG_{5k}$-b-p(HPMA-Bz)$_{17k}$ with different initial drug/polymer ratios at start of their preparation and (C) PM variant $mPEG_{5k}$-b-p(HPMA-Bz)$_{3k}$ with different initial drug/polymer ratios at start of their preparation. Data are presented as mean ± SD of technical repeats (n = 3).

5% PTX loading) is the most stable one in this set by retaining 40% of PTX after 7 days of incubation. At this time point, around 13% of PTX was retained in PM with initial drug/polymer ratio of 0.1 (i.e 10% PTX loading), while almost no PTX was retained in PM with initial drug/polymer ratio of 0.15 (i.e 15% PTX loading) (Fig. 1C).

Monitoring the mean size (presented as hydrodynamic diameter), light-scattering intensity (presented as derived count rate) and size distribution (presented as PDI) of PM at the initial preparation drug/polymer ratio (w/w) of 0.1 pointed to high stability (Fig. 2A–C).

As shown in Fig. 2D, no obvious aggregation could be detected in PM of different polymer variants confirming the stability of the micelles as demonstrated by DLS analysis (Fig. 2A–C).

Besides the 37 °C storage condition, drug-loaded PM were also examined for their stability at 25 and 4 °C for 5 weeks (Fig. S2A to J). The results showed that in lower temperature conditions, the PM were more stable and the PM types had slight impact on PTX stability compared to 37 °C storage condition.

3.3. Evaluation of in vitro release of PTX from PM in presence of Tween 80® and BSA

Besides during storage, PTX release may also occur after administration of the drug loaded PM in the bloodstream. The released PTX molecules will then likely bind to albumin with high protein binding (more than 90%) (Eiseman et al., 1994; Kumar et al., 1993). Previously, the PTX release of PM was studied in PBS using centrifugation method. Utilizing this method, ~30% of the drug was released from PM in 10 days (Shi et al., 2015). To further mimic the *in vivo* situation, PTX release was studied in dispersion medium containing additional 0.2% Tween 80® micelles or 4.5% BSA. Since Tween 80® and mPEG-*b*-p(HPMA-Bz) might form mixed micelles, the stability of the PM in the presence of Tween 80® was investigated using DLS. After 7 days incubation of PM with 0.2% v/v Tween 80® micelles, DLS analysis showed two peaks (Fig. S3), one with a size of around 10 nm (corresponding to Tween 80® micelles) and the other with a size of around 60 nm (corresponding to PM). This indicates that Tween 80® does not disrupt the PM and form mixed micelles with mPEG-*b*-p(HPMA-Bz). This experiment was also performed with PM incubated with PBS/BSA 4.5% w/w and just as with Tween 80®, DLS analysis showed two peaks, which indicates that the BSA did not disrupt the PM (data not shown).

When incubated in one of both media, a fast PTX release (ranging from 36 to 69%, dependent on the PM variant) was seen over the first 4 h followed by a gradual release during the following 7 days (PM prepared at initial drug/polymer ratio of 0.1) (Fig. 3). Independent of the outer medium, the fastest release was obtained with PM based on $mPEG_{5k}$-*b*-p(HPMA-Bz)$_{3k}$ containing the shortest hydrophobic block. By increasing the molecular weight of the hydrophobic block, the drug was released slower. After 7 days, PM based on $mPEG_{5k}$-*b*-p(HPMA-Bz)$_{17k}$ and $mPEG_{5k}$-*b*-p(HPMA-Bz)$_{10k}$ released 72–78% of the loaded drug whereas PM based on $mPEG_{5k}$-*b*-p(HPMA-Bz)$_{5k}$ and $mPEG_{5k}$-*b*-p(HPMA-Bz)$_{3k}$ with the shorter hydrophobic block chains released 81–90% of the loading (Fig. 3A and B).

We also investigated the effect of initial drug/polymer ratio (w/w) on the drug release profile of the different PM variants in 4.5% BSA containing dispersion medium and compared the drug release of PM of polymers $mPEG_{5k}$-*b*-p(HPMA-Bz)$_{17k}$ and $mPEG_{5k}$-*b*-p(HPMA-Bz)$_{3k}$ with different drug/polymer ratio of 0.05, 0.1, and 0.15 (i.e 5%, 10%, and 15% PTX loading). As can be seen in Fig. 4A and B, drug release profiles obtained upon incubation in dispersion medium containing 4.5% BSA were independent of initial drug/polymer ratio for both micellar formulations.

3.4. Effect of type of PM on cellular uptake and tumor penetration

In order to investigate the effect of the size of $mPEG_{5k}$-*b*-p(HPMA-Bz) PM on their uptake by cancer cells, we performed (1) cellular uptake experiments in classical monolayer-grown cell cultures *in vitro* and (2) tumor tissue penetration experiments in 3D tumoroid cultures grown in suspension in ultra-low attachment microplates or in hydrogel matrix.

3.4.1. Effect of size of PM on their uptake by 2D cultured tumor cells

The uptake of Cy3-labeled PM by monolayer culture of PC3 prostate cancer cells and HepG2 hepatocellular carcinoma cells was visualized using confocal laser scanning microscope and quantified with Columbus™ software. Additional endosome labeling with PH Rodo dextran green was applied. Examples of obtained images after two hours incubation with the PM from polymer $mPEG_{5k}$-*b*-p(HPMA-Bz)$_{17k}$ are presented in Fig. 5A. As seen, PM were internalized by both cell types and partially co-localized with the endosomal staining. The different PM displayed a similar uptake pattern. The total fluorescence intensity inside the cells after 4 h of incubation was quantified, normalized by subtraction of baseline fluorescence of non-treated cells and compared (Fig. 5B). While incubation with HepG2 cells seems to lead to somewhat higher cell-associated fluorescence levels compared to PC3, especially in case of smaller PM based on $mPEG_{5k}$-*b*-p(HPMA-Bz)$_{5k}$ and $mPEG_{5k}$-*b*-p(HPMA-Bz)$_{3k}$, PC3 cells did not show substantial uptake differences between the different PM.

3.4.2. Effect of PM size on penetration into 3D tumor tissue cultures

The penetration of $mPEG_{5k}$-*b*-p(HPMA-Bz) of different sizes was studied in two 3D tumor tissue culture systems varying in degree of complexity (HepG2 microspheroids grown in suspension in low attachment Kurarray Elplasia microplate and hydrogel embedded HepG2

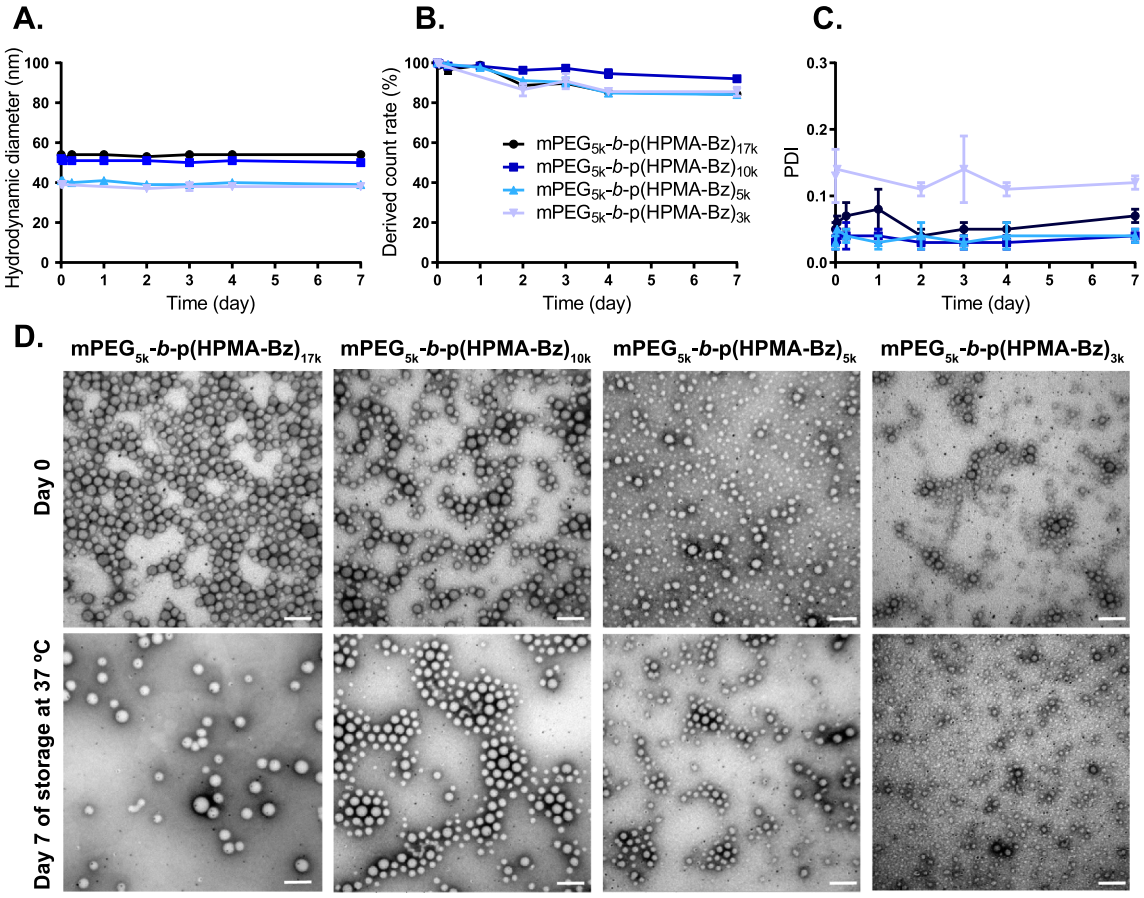

Fig. 2. Stability of the different PTX-loaded PM (initial drug/polymer ratio of 0.1) regarding size (2A), derived count rate (2B), polydispersity (2C), and morphology (2D) during storage in HBS at 37 °C. In the figures A, B and C, data are presented as mean ± SD of independent replicates (n = 3). TEM images were taken immediately after preparation and after 7 days of storage at 37 °C (size bar 100 nm).

3D cultures in Mimetas OrganoPlate®).

PM were incubated with HepG2 microspheroids (diameter approximately 50–100 μm) and imaged with confocal laser scanning microscopy. Representative examples of maximum projection images of acquired Z stacks are presented in Fig. 6. After four hours of incubation with HepG2 microspheroids, the PM of different sizes showed minor differences in penetration profile into the spheroids. Analysis of Cy5 intensity inside the spheroids after four hours of incubation with PM showed slightly lower values for the smaller sized PM based on $mPEG_{5k}$-*b*-p(HPMA-Bz)$_{5k}$ and $mPEG_{5k}$-*b*-p(HPMA-Bz)$_{3k}$ compared to the other two PM variants with larger sizes. In case of PM based on $mPEG_{5k}$-*b*-p(HPMA-Bz)$_{17k}$ penetration kinetics into the spheroids was also studied by live imaging over time. We observed deeper penetration of the Cy5-labeled PM in HepG2 spheroids over time. In the first 1–2 h, the fluorescence signal was mostly detected on the periphery but after 4, 8 and 16 h of incubation the signal was observed in more central parts of the microspheroid.

The ability of PM to passively diffuse into extracellular matrix surrounding tumor cells was studied using Mimetas OrganoPlates®. As shown in Fig. 7, at 4 h, the highest signal at deeper gel layers (400 and 500 μm) was observed for the smaller PM based on $mPEG_{5k}$-b-p(HPMA-Bz)$_{5k}$. However, at 24 h these differences were not detectable anymore

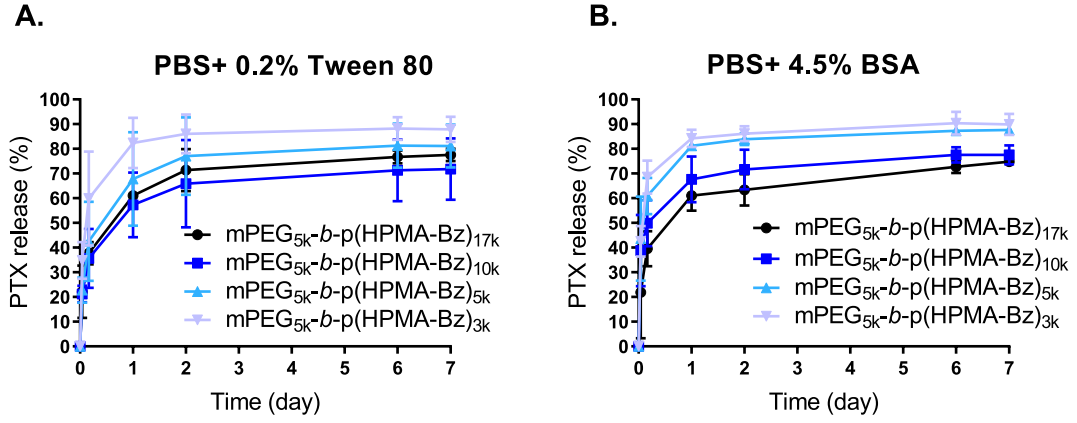

Fig. 3. PTX release from PM based on four different $mPEG_{5k}$-b-p(HPMA-Bz) block copolymers. The release was performed in medium with additionally 0.2% Tween 80® micelles (A) or 4.5% BSA (B) at an initial drug/polymer ratio of 0.1 at 37 °C. Data are presented as mean ± SD of independent replicates (n = 3).

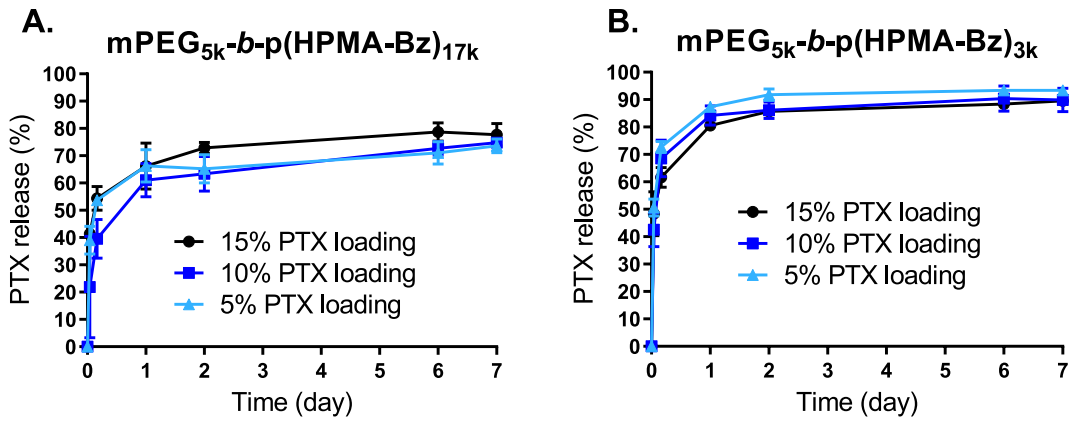

Fig. 4. Release of PTX from PM in PBS with 4.5% BSA at 37 °C (A) polymer $mPEG_{5k}$-b-p(HPMA-Bz)$_{17k}$ with different PTX loadings and (B), polymer $mPEG_{5k}$-b-p(HPMA-Bz)$_{3k}$ with different PTX loadings. Data are presented as mean ± SD of independent replicates (n = 3).

and all three PM formulations except $mPEG_{5k}$-b-p(HPMA-Bz)$_{3k}$ showed approximately the same gel penetration pattern.

4. Discussion

Many PM formulations suffer from physical instability and poor drug retention *in vivo*, which leads to premature drug release. To further improve the entrapment of hydrophobic drugs in PM, PEG block copolymers with a hydrophobic block composed of benzoylated monomers have been developed, and promising results have recently been reported with PM made of $mPEG_{5k}$-*b*-p(HPMA-Bz) and PTX as a prototype hydrophobic anticancer drug (Shi et al., 2015; Shi et al., 2013). In the current study, we optimized this PTX-PM formulation with the aim to better control two main critical design features, namely particle size and drug retention. To that end we varied two parameters, namely the molecular weight of the hydrophobic blocks and drug to polymer ratio in the feed used to prepare the PTX-loaded PM.

Indeed, it is of primary importance to evaluate what the optimal size is for a nanomedicine product and to define the boundaries that a product must remain within to preserve the desired *in vivo* behavior (Bae and Park, 2011). While a nanomedicine for intravenous application should at least be between 10 and 200 nm, with 10 nm being the lower limit to avoid renal filtration (Hoshyar et al., 2016) and 200 nm the upper limit that still theoretically allows for sterile filtration, the vast majority of PM are within the 10–100 nm range (Jones and Leroux, 1999; Yokoyama, 2011). This size range indeed reportedly shows optimal blood residence time and target localization in tumors. However, previous research revealed that nanoparticles must be below 50 nm in order to sufficiently penetrate into tumors (Cabral et al., 2011). We showed here that our PM can be sized down to below 40 nm while preserving their very low polydispersity index. Here, the largest two blocks led to a 52 nm particle while the smallest two blocks resulted in particles of still around 39 nm in diameter.

Although we did not observe any substantial differences in the cellular uptake of the PM in 2D and 3D microspheroids, an increased penetration of the smaller PM was seen in human hepatocellular tumors cultured in extracellular matrix in 4 h. This is in line with previous studies on the effect of size on tumor penetration (Cabral et al., 2011; Priwitaningrum et al., 2016). PM with a size of 40 nm based on $mPEG_{5k}$-b-p(HPMA-Bz)$_{5k}$ showed the best penetration at each depth layer in the culture. Interestingly, though similar in size, the PM based on $mPEG_{5k}$-*b*-p(HPMA-Bz)$_{3k}$ lost its penetration capacity, which can probably be attributed to low stability of these PM in biological media.

Following size, the second key quality attribute is drug release rate, as this determines the concentration-time profile of free active drug at the target site. While this is in the first place likely determined by the PM core size and hydrophobicity, and thus by the hydrophobic polymer block length, the initial loading (which in turn is determined by the drug to polymer ratio in the feed solution used for preparation of the micelles) is an influential composition parameter as well, as shown by Yu et al. (2013). Literature reveals on the one hand that very slow drug release leads to suboptimal pharmacologic activity while on the other hand fast release kinetics prevents the drug from reaching the target site (Yokoyama, 2014). Slow but sustained drug release is typically

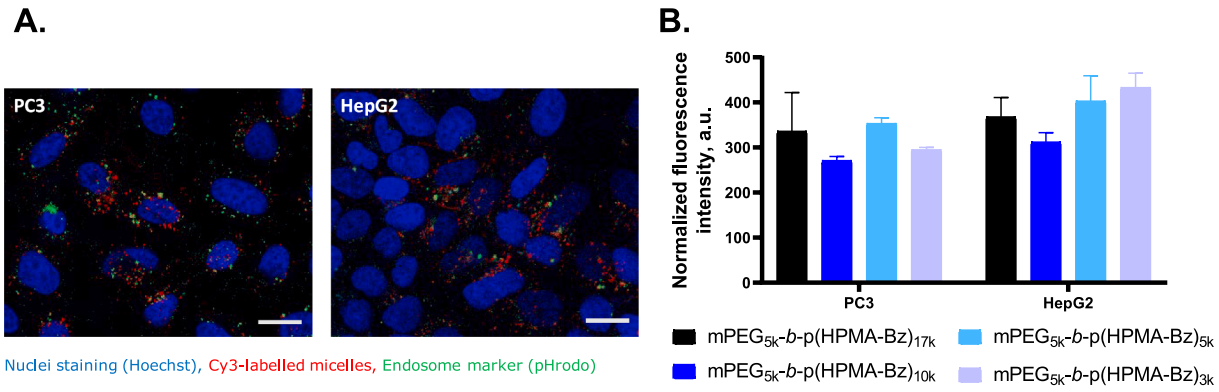

Fig. 5. PM uptake by PC3 and HepG2 cells in monolayer cultures *in vitro*: (A) Representative confocal microscopy images of Cy3-labeled PM based on $mPEG_{5k}$-b-p(HPMA-Bz)$_{17k}$ after 2 h incubation with PC3 and HepG2 cells; Red: PM label, blue: nuclei stained with Hoechst 33342, and green: endosomes labeled with pHrodo™ green; size bar 10 μm. (B) Cell-associated fluorescence intensity after 4 h with different $mPEG_{5k}$-b-p(HPMA-Bz) PM. Normalized by subtraction of baseline fluorescence of non-treated cells; each bar represents an average cell-associated fluorescence intensity. Data are presented as mean ± SD of independent replicates (n = 3). (For interpretation of the references to colour in this figure legend, the reader is referred to the web version of this article.)

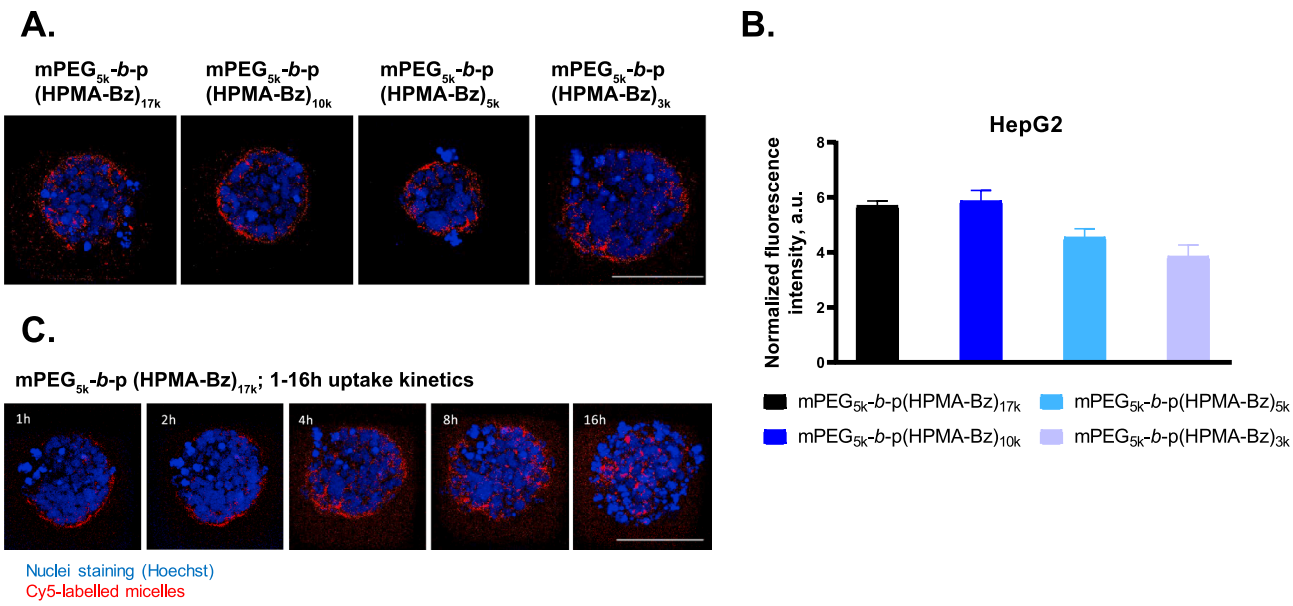

Fig. 6. PM penetration into HepG2 microspheroids: (A) Representative confocal microscopy images of Cy5-labeled PM after 4 h of incubation with HepG2 microspheroids at 37 °C; (B) Bar chart depicting Cy5 fluorescence intensity detected in the microspheroids after 4 h of incubation with PM and normalized by subtraction of baseline fluorescence of non-treated wells; each bar represents fluorescence intensity. Data are presented as mean ± SD of independent replicates (n = 3); (C) Representative confocal microscopy images of penetration kinetics of $mPEG_{5k}$-b-p(HPMA-Bz)$_{17k}$ PM; Red: PM label, blue: nuclei stained with Hoechst 33342, size bar 100 μm. (For interpretation of the references to colour in this figure legend, the reader is referred to the web version of this article.)

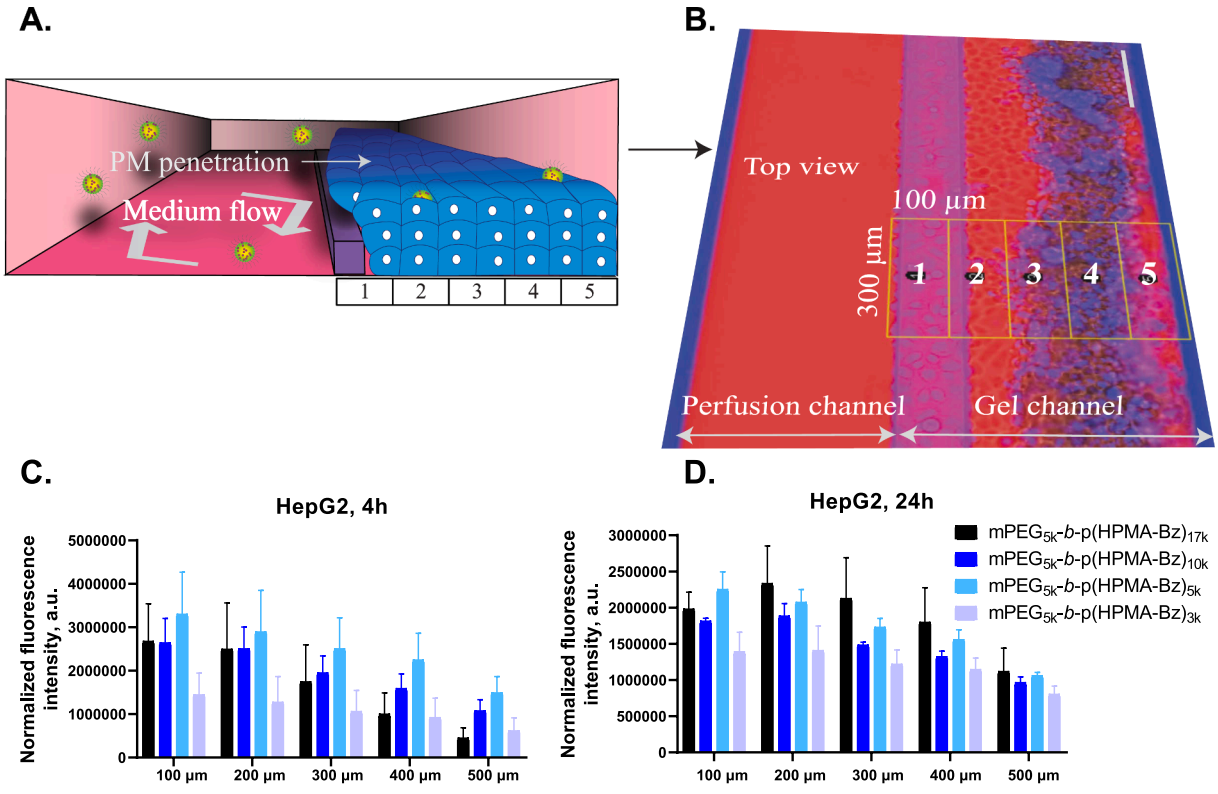

Fig. 7. PM penetration in gel embedded HepG2 3D cultures: (A) schematic view of PM penetration in HepG2 cells seeded in OrganoPlate® (B) top view; an example of confocal microscopy image of gel embedded HepG2 in OrganoPlate® after 4 h of incubation with Cy3-labeled PM. It shows channels geometry of the OrganoPlate® and image fields used for Cy3 intensity analysis. Red: PM label, blue: nuclei stained with Hoechst 33342, size bar 200 μm; (C) and (D) Bar chart depicting Cy3 fluorescence intensity detected in the 300 by 100 μm regions of the gel (same regions in each image) after 4 h (C) and 24 h (D) of continued perfusion of PM through the medium channel. Normalized by subtraction of baseline fluorescence of non-treated cells; each bar represents an average cell-associated fluorescence intensity. Data are presented as mean ± SD of independent replicates (n = 3). (For interpretation of the references to colour in this figure legend, the reader is referred to the web version of this article.)

aimed at and Abouelmagd et al. reviewed several reports on a range of different PTX nano-formulations that show sustained drug release independent of formulation type (Abouelmagd et al., 2015). Meanwhile, in cancer therapy, it can be beneficial if the drug is rapidly released from PM as soon as it has reached the tumor. Rapid drug release can result in improved therapeutic efficacy and preventing tumor cells to acquire resistance to the drug (Deng et al., 2012).

In our study we showed that the presence of longer hydrophobic blocks in the PM core results in a better retention and a slower release rate of PTX over time, which are in line with other studies (Hussein and Youssry, 2018; Lin et al., 2003). Interestingly, we do not observe a correlation between initial drug loading and drug release rate. To perform the release tests, Tween 80®/PBS and BSA/PBS were used as the release media. The addition of excess amounts of Tween 80® and BSA helped to better represent the *in vivo* release. However, PTX release profile showed no substantial differences in these two media. Moreover, we evaluated the released fraction of the PTX indirectly, through quantifying the remaining drug in the PM at regular time points. All our PM formulations showed evident fast release (between 36 and 69% of the loading) within the first 4 h. Whether this is a desirable release pattern depends on the time that PM after iv administration significantly accumulate in tumors exploiting the EPR effect (Maeda et al., 2013).

Regarding the PTX loading percentages, it has been previously shown that lower drug loadings result in a better stability (Lübtow et al., 2019). Here, we observed that the relatively high initial drug loading of 15% w/w was clearly the least stable. Although PM with a lowest initial drug loading of 5% w/w in our study showed better stability upon storage, no substantial differences in the *in vitro* drug release profile were observed between the initial drug loading of 5 and the intermediate 10% w/w. Taking into account the practical advantages of higher drug loading, an initial drug loading of 10% w/w will be selected for further development.

5. Conclusion

In this study, we aimed to optimize a novel PTX-PM anticancer drug product and select a lead candidate formulation of this product for further clinical development. To this end, we formulated PTX-PM and performed advanced *in vitro* tests looking at stability, drug release in the presence of Tween 80® and BSA as solubilizers and PM tumor penetration in cell cultures, the latter two assays being more predictive of *in vivo* behavior. In these assays, we observed that the PM obtained with the two largest block copolymers $mPEG_{5k}$-*b*-$p(HPMA\text{-}Bz)_{17k}$ and $mPEG_{5k}$-*b*-$p(HPMA\text{-}Bz)_{10k}$ have similar size, stability, PTX retention and release profile as well as cellular uptake and penetration. Meanwhile, PM of the two smallest block copolymers $mPEG_{5k}$-*b*-$p(HPMA\text{-}Bz)_{5k}$ and $mPEG_{5k}$-*b*-$p(HPMA\text{-}Bz)_{3k}$ revealed a similar but smaller size, and also a faster leakage of which the smallest, namely $mPEG_{5k}$-*b*-$p(HPMA\text{-}Bz)_{3k}$ polymer showed inferior stability and decreased cellular uptake. Since PTX retention and tumor penetration are both desirable features that are apparently at odds with each other, utilizing $mPEG_{5k}$-*b*-$p(HPMA\text{-}Bz)_{17k}$ and $mPEG_{5k}$-*b*-$p(HPMA\text{-}Bz)_{5k}$ polymers would provide the better stability of the PM based on the former and smaller size and better penetration property of the PM based on the latter polymer and consequently, we can efficiently choose the one optimum polymer with help of further *in vivo* studies. In light of future studies, the results obtained in the current project can pave the way towards developing more efficient systems for drug delivery.

CRediT authorship contribution statement

Maryam Sheybanifard: Investigation, Writing - original draft, Writing - review & editing. **Nataliia Beztsinna:** Investigation, Writing - original draft, Writing - review & editing. **Mahsa Bagheri:** Investigation. **Eva Miriam Buhl:** Investigation. **Jaleesa Bresseleers:** Investigation. **Aida Varela-Moreira:** Investigation. **Yang Shi:** Writing - review & editing. **Cornelus F. Nostrum:** Writing - review & editing. **Gabri Pluijm:** Writing - review & editing, Funding acquisition. **Gert Storm:** Writing - review & editing, Funding acquisition, Supervision. **Wim E. Hennink:** Writing - review & editing, Supervision. **Twan Lammers:** Writing - review & editing, Funding acquisition, Supervision. **Josbert M. Metselaar:** Writing - review & editing, Supervision, Funding acquisition.

Declaration of Competing Interest

The authors declare that they have no known competing financial interests or personal relationships that could have appeared to influence the work reported in this paper.

Acknowledgments

This work was supported by the Dutch Cancer Society (KWF)-Alpe D'Huzes (UL2014-7058) entitled 'Near-patient' prostate cancer models for the assessment of disease prognosis and therapy response'(PROPER) and also by the Deutsche Forschungsgemeinschaft (DFG) in the framework of the Research Training Group 2375 "Tumor-targeted Drug Delivery" grant 331065168.

Appendix A. Supplementary material

Supplementary data to this article can be found online at https://doi.org/10.1016/j.ijpharm.2020.119409.

References

Abouelmagd, S.A., Sun, B., Chang, A.C., Ku, Y.J., Yeo, Y., 2015. Release kinetics study of poorly water-soluble drugs from nanoparticles: are we doing it right? Mol. Pharm. 12, 997–1003.
Adams, J.D., Flora, K., Goldspiel, B., Wilson, J., Arbuck, S., Finley, R., 1993. Taxol: a history of pharmaceutical development and current pharmaceutical concerns. J. Natl. Cancer Inst. Monographs 141–147.
Bader, H., Ringsdorf, H., Schmidt, B., 1984. Watersoluble polymers in medicine. Die Angewandte Makromolekulare Chemie: Appl. Macromol. Chem. Phys. 123, 457–485.
Bae, Y.H., Park, K., 2011. Targeted drug delivery to tumors: myths, reality and possibility. J. Control. Release 153, 198.
Bagheri, M., Bresseleers, J., Varela-Moreira, A., Sandre, O., Meeuwissen, S.A., Schiffelers, R.M., Metselaar, J.M., Van Nostrum, C.F., van Hest, J.C., Hennink, W.E., 2018. Effect of formulation and processing parameters on the size of mPEG-b-p (HPMA-Bz) polymeric micelles. Langmuir 34, 15495–15506.
Blum, J., Savin, M., Edelman, G., Pippen, J., Robert, N., Sandbach, J., Carrasco, S., O'Shaughnessy, J., 2004. Long term disease control in taxane-refractory metastatic breast cancer treated with nab paclitaxel. J. Clin. Oncol. 22 543-543.
Cabral, H., Matsumoto, Y., Mizuno, K., Chen, Q., Murakami, M., Kimura, M., Terada, Y., Kano, M., Miyazono, K., Uesaka, M., 2011. Accumulation of sub-100 nm polymeric micelles in poorly permeable tumours depends on size. Nat. Nanotechnol. 6, 815–823.
Cabral, H., Miyata, K., Osada, K., Kataoka, K., 2018. Block copolymer micelles in nanomedicine applications. Chem. Rev. 118, 6844–6892.
Chauhan, V.P., Stylianopoulos, T., Martin, J.D., Popović, Z., Chen, O., Kamoun, W.S., Bawendi, M.G., Fukumura, D., Jain, R.K., 2012. Normalization of tumour blood vessels improves the delivery of nanomedicines in a size-dependent manner. Nat. Nanotechnol. 7, 383–388.
Cooney, R., Kappock, T., Pung, A., Bertram, J., 1993. Solubilization, cellular uptake, and activity of beta-carotene and other carotenoids as inhibitors of neoplastic transformation in cultured cells. Methods Enzymol. 214, 55–68.
Cragg, G.M., 1998. Paclitaxel (Taxol®): a success story with valuable lessons for natural product drug discovery and development. Med. Res. Rev. 18, 315–331.
Deng, C., Jiang, Y., Cheng, R., Meng, F., Zhong, Z., 2012. Biodegradable polymeric micelles for targeted and controlled anticancer drug delivery: promises, progress and prospects. Nano Today 7, 467–480.
Desai, N., Trieu, V., Yao, Z., Louie, L., Ci, S., Yang, A., Tao, C., De, T., Beals, B., Dykes, D., 2006. Increased antitumor activity, intratumor paclitaxel concentrations, and endothelial cell transport of cremophor-free, albumin-bound paclitaxel, ABI-007, compared with cremophor-based paclitaxel. Clin. Cancer Res. 12, 1317–1324.
Eiseman, J.L., Eddington, N.D., Leslie, J., MacAuley, C., Sentz, D.L., Zuhowski, M., Kujawa, J.M., Young, D., Egorin, M.J., 1994. Plasma pharmacokinetics and tissue distribution of paclitaxel in CD 2 F 1 mice. Cancer Chemother. Pharmacol. 34, 465–471.
Fang, J., Nakamura, H., Maeda, H., 2011. The EPR effect: unique features of tumor blood vessels for drug delivery, factors involved, and limitations and augmentation of the

effect. Adv. Drug Deliv. Rev. 63, 136–151.
Finley, R.S., Rowinsky, E.K., 1994. Patient care issues: the management of paclitaxel-related toxicities. Ann. Pharmacother. 28, S27–S30.
Gelderblom, H., Verweij, J., Nooter, K., Sparreboom, A., 2001. Cremophor EL: the drawbacks and advantages of vehicle selection for drug formulation. Eur. J. Cancer 37, 1590–1598.
Gothwal, A., Khan, I., Gupta, U., 2016. Polymeric micelles: recent advancements in the delivery of anticancer drugs. Pharm. Res. 33, 18–39.
Guideline, I.H.T., 2005. Impurities: Guideline for residual solvents Q3C (R5). Current Step 4, 1–25.
Hamaguchi, T., Matsumura, Y., Suzuki, M., Shimizu, K., Goda, R., Nakamura, I., Nakatomi, I., Yokoyama, M., Kataoka, K., Kakizoe, T., 2005. NK105, a paclitaxel-incorporating micellar nanoparticle formulation, can extend in vivo antitumour activity and reduce the neurotoxicity of paclitaxel. Br. J. Cancer 92, 1240.
Hoshyar, N., Gray, S., Han, H., Bao, G., 2016. The effect of nanoparticle size on in vivo pharmacokinetics and cellular interaction. Nanomedicine 11, 673–692.
Hussein, Y.H., Youssry, M., 2018. Polymeric micelles of biodegradable diblock copolymers: enhanced encapsulation of hydrophobic drugs. Materials 11, 688.
Ibrahim, N.K., Desai, N., Legha, S., Soon-Shiong, P., Theriault, R.L., Rivera, E., Esmaeli, B., Ring, S.E., Bedikian, A., Hortobagyi, G.N., 2002. Phase I and pharmacokinetic study of ABI-007, a Cremophor-free, protein-stabilized, nanoparticle formulation of paclitaxel. Clin. Cancer Res. 8, 1038–1044.
Jones, M.-C., Leroux, J.-C., 1999. Polymeric micelles–a new generation of colloidal drug carriers. Eur. J. Pharm. Biopharm. 48, 101–111.
Jordan, M.A., Wendell, K., Gardiner, S., Derry, W.B., Copp, H., Wilson, L., 1996. Mitotic block induced in HeLa cells by low concentrations of paclitaxel (Taxol) results in abnormal mitotic exit and apoptotic cell death. Cancer Res. 56, 816–825.
Kataoka, K., Matsumoto, T., Yokoyama, M., Okano, T., Sakurai, Y., Fukushima, S., Okamoto, K., Kwon, G.S., 2000. Doxorubicin-loaded poly (ethylene glycol)–poly (β-benzyl-l-aspartate) copolymer micelles: their pharmaceutical characteristics and biological significance. J. Control. Release 64, 143–153.
Kim, J.H., Emoto, K., Iijima, M., Nagasaki, Y., Aoyagi, T., Okano, T., Sakurai, Y., Kataoka, K., 1999. Core-stabilized polymeric micelle as potential drug carrier: increased solubilization of taxol. Polym. Adv. Technol. 10, 647–654.
Kim, S.C., Kim, D.W., Shim, Y.H., Bang, J.S., Oh, H.S., Kim, S.W., Seo, M.H., 2001. In vivo evaluation of polymeric micellar paclitaxel formulation: toxicity and efficacy. J. Control. Release 72, 191–202.
Kim, T.-Y., Kim, D.-W., Chung, J.-Y., Shin, S.G., Kim, S.-C., Heo, D.S., Kim, N.K., Bang, Y.-J., 2004. Phase I and pharmacokinetic study of Genexol-PM, a cremophor-free, polymeric micelle-formulated paclitaxel, in patients with advanced malignancies. Clin. Cancer Res. 10, 3708–3716.
Kumar, G., Walle, U., Bhalla, K., Walle, T., 1993. Binding of taxol to human plasma, albumin and alpha 1-acid glycoprotein. Res. Commun. Chem. Pathol. Pharmacol. 80, 337–344.
Letchford, K., Liggins, R., Wasan, K.M., Burt, H., 2009. In vitro human plasma distribution of nanoparticulate paclitaxel is dependent on the physicochemical properties of poly (ethylene glycol)-block-poly (caprolactone) nanoparticles. Eur. J. Pharm. Biopharm. 71, 196–206.
Lin, W.-J., Juang, L.-W., Lin, C.-C., 2003. Stability and release performance of a series of pegylated copolymeric micelles. Pharm. Res. 20, 668–673.
Lu, Y., Park, K., 2013. Polymeric micelles and alternative nanonized delivery vehicles for poorly soluble drugs. Int. J. Pharm. 453, 198–214.
Lübtow, M.M., Haider, M.S., Kirsch, M., Klisch, S., Luxenhofer, R., 2019. Like dissolves like? A comprehensive evaluation of partial solubility parameters to predict polymer-drug compatibility in ultrahigh drug-loaded polymer micelles. Biomacromolecules 20, 3041–3056.
Maeda, H., Nakamura, H., Fang, J., 2013. The EPR effect for macromolecular drug delivery to solid tumors: Improvement of tumor uptake, lowering of systemic toxicity, and distinct tumor imaging in vivo. Adv. Drug Deliv. Rev. 65, 71–79.
Miller, T., Breyer, S., van Colen, G., Mier, W., Haberkorn, U., Geissler, S., Voss, S., Weigandt, M., Goepferich, A., 2013. Premature drug release of polymeric micelles and its effects on tumor targeting. Int. J. Pharm. 445, 117–124.
Naksuriya, O., Shi, Y., Van Nostrum, C.F., Anuchapreeda, S., Hennink, W.E., Okonogi, S., 2015. HPMA-based polymeric micelles for curcumin solubilization and inhibition of cancer cell growth. Eur. J. Pharm. Biopharm. 94, 501–512.
Nasongkla, N., Bey, E., Ren, J., Ai, H., Khemtong, C., Guthi, J.S., Chin, S.-F., Sherry, A.D., Boothman, D.A., Gao, J., 2006. Multifunctional polymeric micelles as cancer-targeted, MRI-ultrasensitive drug delivery systems. Nano Lett. 6, 2427–2430.
Nishiyama, N., Matsumura, Y., Kataoka, K., 2016. Development of polymeric micelles for targeting intractable cancers. Cancer Sci. 107, 867–874.
Peltier, S., Oger, J.-M., Lagarce, F., Couet, W., Benoît, J.-P., 2006. Enhanced oral paclitaxel bioavailability after administration of paclitaxel-loaded lipid nanocapsules. Pharm. Res. 23, 1243–1250.
Pratten, M.K., Lloyd, J.B., Hörpel, G., Ringsdorf, H., 1985. Micelle-forming block copolymers: pinocytosis by macrophages and interaction with model membranes. Die Makromolekulare Chemie: Macromol. Chem. Phys. 186, 725–733.
Priwitaningrum, D.L., Blondé, J.-B.G., Sridhar, A., van Baarlen, J., Hennink, W.E., Storm, G., Le Gac, S., Prakash, J., 2016. Tumor stroma-containing 3D spheroid arrays: a tool to study nanoparticle penetration. J. Control. Release 244, 257–268.
Quock, J., Dea, G., Tanaka, M., Gandara, D., Lara, P., Lau, D., 2002. Premedication strategy for weekly paclitaxel. Cancer Invest. 20, 666–672.
Shi, Y., Lammers, T., Storm, G., Hennink, W.E., 2017. Physico-chemical strategies to enhance stability and drug retention of polymeric micelles for tumor-targeted drug delivery. Macromol. Biosci. 17, 1600160.
Shi, Y., Van Der Meel, R., Theek, B., Oude Blenke, E., Pieters, E.H., Fens, M.H., Ehling, J., Schiffelers, R.M., Storm, G., Van Nostrum, C.F., 2015. Complete regression of xenograft tumors upon targeted delivery of paclitaxel via Π-Π stacking stabilized polymeric micelles. ACS Nano 9, 3740–3752.
Shi, Y., van Steenbergen, M.J., Teunissen, E.A., Novo, L.S., Gradmann, S., Baldus, M., van Nostrum, C.F., Hennink, W.E., 2013. Π-Π stacking increases the stability and loading capacity of thermosensitive polymeric micelles for chemotherapeutic drugs. Biomacromolecules 14, 1826–1837.
Shiraishi, K., Yokoyama, M., 2013. Polymeric micelles possessing polyethyleneglycol as outer shell and their unique behaviors in accelerated blood clearance phenomenon. Biol. Pharm. Bull. 36, 878–882.
Shuai, X., Merdan, T., Schaper, A.K., Xi, F., Kissel, T., 2004. Core-cross-linked polymeric micelles as paclitaxel carriers. Bioconjug. Chem. 15, 441–448.
Soga, O., van Nostrum, C.F., Fens, M., Rijcken, C.J., Schiffelers, R.M., Storm, G., Hennink, W.E., 2005. Thermosensitive and biodegradable polymeric micelles for paclitaxel delivery. J. Control. Release 103, 341–353.
Talelli, M., Barz, M., Rijcken, C.J., Kiessling, F., Hennink, W.E., Lammers, T., 2015. Core-crosslinked polymeric micelles: principles, preparation, biomedical applications and clinical translation. Nano Today 10, 93–117.
Talelli, M., Iman, M., Varkouhi, A.K., Rijcken, C.J., Schiffelers, R.M., Etrych, T., Ulbrich, K., van Nostrum, C.F., Lammers, T., Storm, G., 2010. Core-crosslinked polymeric micelles with controlled release of covalently entrapped doxorubicin. Biomaterials 31, 7797–7804.
Talelli, M., Rijcken, C.J., Hennink, W.E., Lammers, T., 2012. Polymeric micelles for cancer therapy: 3 C's to enhance efficacy. Curr. Opin. Solid State Mater. Sci. 16, 302–309.
Torchilin, V.P., 2007. Micellar nanocarriers: pharmaceutical perspectives. Pharm. Res. 24, 1.
Trietsch, S.J., Naumovska, E., Kurek, D., Setyawati, M.C., Vormann, M.K., Wilschut, K.J., Lanz, H.L., Nicolas, A., Ng, C.P., Joore, J., 2017. Membrane-free culture and real-time barrier integrity assessment of perfused intestinal epithelium tubes. Nat. Commun. 8, 262.
van Nostrum, C.F., 2011. Covalently cross-linked amphiphilic block copolymer micelles. Soft Matter 7, 3246–3259.
van Zuylen, L., Verweij, J., Sparreboom, A., 2001. Role of formulation vehicles in taxane pharmacology. Invest. New Drugs 19, 125–141.
Wevers, N.R., Van Vught, R., Wilschut, K.J., Nicolas, A., Chiang, C., Lanz, H.L., Trietsch, S.J., Joore, J., Vulto, P., 2016. High-throughput compound evaluation on 3D networks of neurons and glia in a microfluidic platform. Sci. Rep. 6, 38856.
Yokoyama, M., 2011. Clinical applications of polymeric micelle carrier systems in chemotherapy and image diagnosis of solid tumors. J. Exp. Clin. Med. 3, 151–158.
Yokoyama, M., 2014. Polymeric micelles as drug carriers: their lights and shadows. J. Drug Target. 22, 576–583.
Yoo, H.S., Park, T.G., 2001. Biodegradable polymeric micelles composed of doxorubicin conjugated PLGA–PEG block copolymer. J. Control. Release 70, 63–70.
Yu, H., Xia, D., Zhu, Q., Zhu, C., Chen, D., Gan, Y., 2013. Supersaturated polymeric micelles for oral cyclosporine A delivery. Eur. J. Pharm. Biopharm. 85, 1325–1336.
Zhuang, W.-R., Wang, Y., Cui, P.-F., Xing, L., Lee, J., Kim, D., Jiang, H.-L., Oh, Y.-K., 2019. Applications of π-π stacking interactions in the design of drug-delivery systems. J. Control. Release 294, 311–326.